Capacity Investigation of Brine-Bearing Sands of the Frio Formation for Geologic Sequestration of CO_2

Christine Doughty (cadoughty@lbl.gov; 510-486-6453)
Karsten Pruess (k_pruess@lbl.gov; 510-486-6732)
Sally M. Benson (smbenson@lbl.gov; 510-486-5875)
Lawrence Berkeley National Laboratory
1 Cyclotron Rd, MS 90-1116
Berkeley, CA 94720

Susan D. Hovorka (susan.hovorka@beg.utexas.edu; 512-471-4863)
Paul R. Knox (paul.knox@beg.utexas.edu; 512-471-7313)
Bureau of Economic Geology
P.O. Box X, The University of Texas
Austin, TX 78713

Christopher T. Green (ctgreen@ucdavis.edu; 530-752-1372)
University of California, Hydrologic Sciences
1 Shields Ave.
Davis, CA 95616

Abstract

The capacity of fluvial brine-bearing formations to sequester CO_2 is investigated using numerical simulations of CO_2 injection and storage. Capacity is defined as the volume fraction of the subsurface available for CO_2 storage and is conceptualized as a product of factors that account for two-phase flow and transport processes, formation geometry, formation heterogeneity, and formation porosity. The space and time domains used to define capacity must be chosen with care to obtain meaningful results, especially when comparing different authors' work. Physical factors that impact capacity include permeability anisotropy and relative permeability to CO_2, brine/CO_2 density and viscosity ratios, the shape of the trapping structure, formation porosity and the presence of low-permeability layering.

Introduction

Geologic sequestration of CO_2 in brine-bearing formations has been proposed as a means of reducing the atmospheric load of greenhouse gases. For this procedure to have any meaningful impact on the global carbon cycle, vast quantities of CO_2 must be injected into the subsurface and isolated from the biosphere for hundreds or thousands of years. We use numerical simulations to investigate the capacity of deep brine-saturated formations to sequester CO_2 that has been compressed to a supercritical state. The three-dimensional (3D) model includes all flow and transport processes relevant for a two-

phase (liquid-gas), three-component (CO_2, water, dissolved NaCl) system. In particular, CO_2 may exist in a gas-like supercritical state or be dissolved in the aqueous phase. Salt may precipitate out of the brine, but the rock matrix itself is inert. Thus, chemical reactions between CO_2 and rock minerals that could potentially contribute to mineral trapping of CO_2 are not considered. The model includes heterogeneity representative of a fluvial geologic setting in which permeability varies by nearly six orders of magnitude, making preferential flow a significant effect as well.

Of the numerous brine-bearing formations that have been identified as having potential for geologic sequestration of CO_2 (Hovorka et al., 2000), we focus on the Frio formation of the upper Texas Gulf Coast. Key features that make the Frio formation well-suited for geologic sequestration include the existence of many localized CO_2 point sources (power plants, refineries, chemical plants), large volumes of suitable brine formations (unusable as potable water, away from petroleum resources), formations that are well characterized due to stratigraphically and structurally analogous petroleum reservoirs, extensive use of the Frio for deep well injection of hazardous waste, and CO_2 injection technology developed for improved oil recovery that has been tested in analogous Gulf Coast formations.

Definition of Capacity

No single, well-accepted definition of capacity exists. We define capacity C as the volume fraction of the subsurface within a defined stratigraphic interval available for CO_2 sequestration. We construct C as the product of four factors:

$$C = C_i \cdot C_g \cdot C_h \cdot \phi. \quad (1)$$

C_i is intrinsic capacity, which is controlled by multi-phase flow and transport phenomena; C_g is geometric capacity factor, which is controlled by formation geometry; C_h is heterogeneity capacity factor, which is controlled by geologic variability; and ϕ is porosity, the fraction of void space within the formation. We have found this formulation useful for investigating the different processes that influence C and comparing our work to that of other authors, but in practice, one may not be able to separately calculate C_i, C_g, and C_h.

Intrinsic Capacity C_i

Intrinsic capacity C_i is defined as the fraction of pore space occupied by CO_2 assuming radial flow through a uniform medium. C_i can be divided into gas- and liquid-phase components: $C_i = C_{ig} + C_{il}$. A Buckley-Leverett type analysis (Buckley and Leverett, 1942; Pruess et al., 2001) gives

$$C_{ig} \cong S_g, \quad (2)$$

where S_g is the average gas saturation behind the front (the small contribution of water vapor to S_g has been neglected).

For CO_2 dissolved in the aqueous phase,

$$C_{il} = S_l X_l^{CO_2} \rho_l / \rho_g, \quad (3)$$

where S_l and $X_l^{CO_2}$ are the saturation and CO_2 mass fraction, respectively, averaged over the liquid (aqueous) phase behind the front and ρ_l/ρ_g is the liquid/gas density ratio. Inclusion of the ρ_l/ρ_g term makes C_{il} the volume fraction that CO_2 dissolved in the liquid phase would occupy if it were converted to the gas phase. This formulation ensures that intrinsic capacity is additive between gas and aqueous phases, regardless of the phase partitioning of CO_2, which depends strongly on pressure-temperature conditions.

Geometric Capacity Factor C_g

Geometric capacity factor C_g accounts for departures from the idealized radial flow geometry assumed for intrinsic capacity, such as partially penetrating injection wells, gravity segregation, and dipping formations with spill points. Figures 1a and 1b illustrate the effect of partial penetration and gravity on CO_2 plume development in a homogeneous medium.

Heterogeneity Capacity Factor C_h

Heterogeneity capacity factor C_h accounts for bypass flow arising from geologic heterogeneity, as illustrated in Figure 1c. This factor has been referred to as horizontal sweep efficiency in the petroleum literature.

Calculating Capacity Factors

For non-radial flow or a heterogeneous medium, there may not be a single CO_2 front. We extend the definitions of C_{ig} and C_{il} given in Equations (2) and (3) to

$$C_{ig} \cdot C_g \cdot C_h = \langle S_g \rangle, \quad (4)$$

$$C_{il} \cdot C_g \cdot C_h = \langle S_l X_l^{CO_2} \rho_l / \rho_g \rangle, \quad (5)$$

where $\langle\rangle$ identifies the region of space over which averages are taken. Examples of averaging regions include the volume of a natural CO_2 trap (defined by the distance from the injection well to a spill point or cap rock discontinuity), the volume of a targeted geologic formation, or some relevant unit volume (e.g., 1 km^3 around a power plant). Obviously, the choice of averaging region can have a large effect on the capacity value

calculated, so it must be chosen carefully to ensure meaningful comparison of different scenarios.

The stage of CO_2 plume development at which capacity is calculated is also important. Averages may be taken when the boundary of the averaging region is first encountered or, alternatively, when quasi-steady flow conditions exist throughout the averaging region.

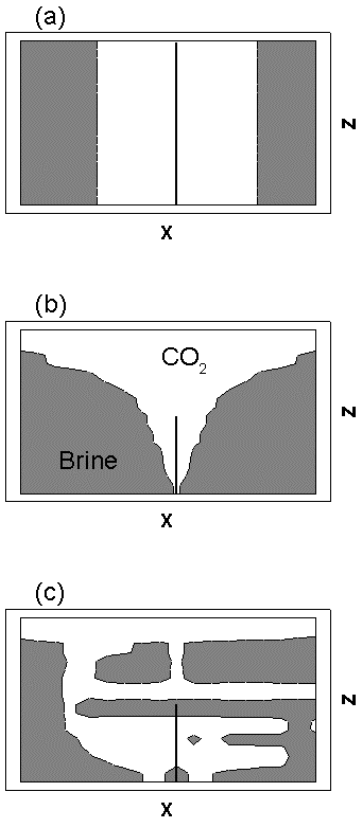

Figure 1. Schematic representations of CO_2 injection for (a) a uniform medium with no gravity, (b) a uniform medium with gravity, and (c) a heterogeneous medium with gravity.

Methods

Numerical Simulator TOUGH2

TOUGH2 is a general-purpose numerical simulator for multiphase flows in porous and fractured media. It employs a multiphase extension of Darcy's law that includes relative permeability and capillary-pressure effects and incorporates accurate phase-partitioning and thermophysical properties of water-CO_2-NaCl mixtures for supercritical CO_2. The present simulations are relatively short-term (less than 60 years), so they emphasize advective processes. Slower processes such as liquid-phase diffusion of dissolved species and the buoyancy effect of CO_2 dissolved in water are neglected. Further details of the TOUGH2 simulator may be found in a companion paper (Hovorka et al., 2001 and references therein), and in the user's guide itself (Pruess et al., 1999). The treatment used for thermophysical properties in the water-CO_2-NaCl system is presented in Pruess and Garcia (2001).

Cedar Bayou Model

We developed a numerical model of a 1 km by 1 km by 100 m region of the Frio formation underlying the Cedar Bayou power plant near Houston. Formation heterogeneities are described by transition probability geostatistics (Carle, 1996; Fogg et al., 2001), using a well log study from the nearby Umbrella Point reservoir (Vining, 1997) and an overall understanding of the fluvial-deltaic depositional structures of the Frio formation (Galloway, 1982). A cut-away 3D view of the model is shown in Figure 2. Each of the ten layers represents one of three different depositional settings: interdistributary bayfill (mostly low-permeability shale and splays, some intermediate-permeability channels), barrier bars (mostly high-permeability sand), or distributary channels (mostly intermediate-permeability channels and splays, some shale). Further details of model development and additional references are described in a companion paper (Hovorka et al., 2001 and references therein). Model properties are summarized in Table 1.

The boundary and initial conditions assumed for the model are as follows. The top and bottom boundaries are closed, representing low-permeability sealing layers. The lateral boundaries are open, and are used to represent the spill point of the storage volume. Supercritical CO_2 is injected into a single well open over the lower half of model. Injection rate is a constant 21.6 kg/s, which is partitioned among the various layers in proportion to the permeability-thickness product of the layer. Initial conditions consist of a hydrostatic pressure profile for brine with TDS content of 100,000 ppm and a constant temperature of 78^{o}C (average pressure 188 bars).

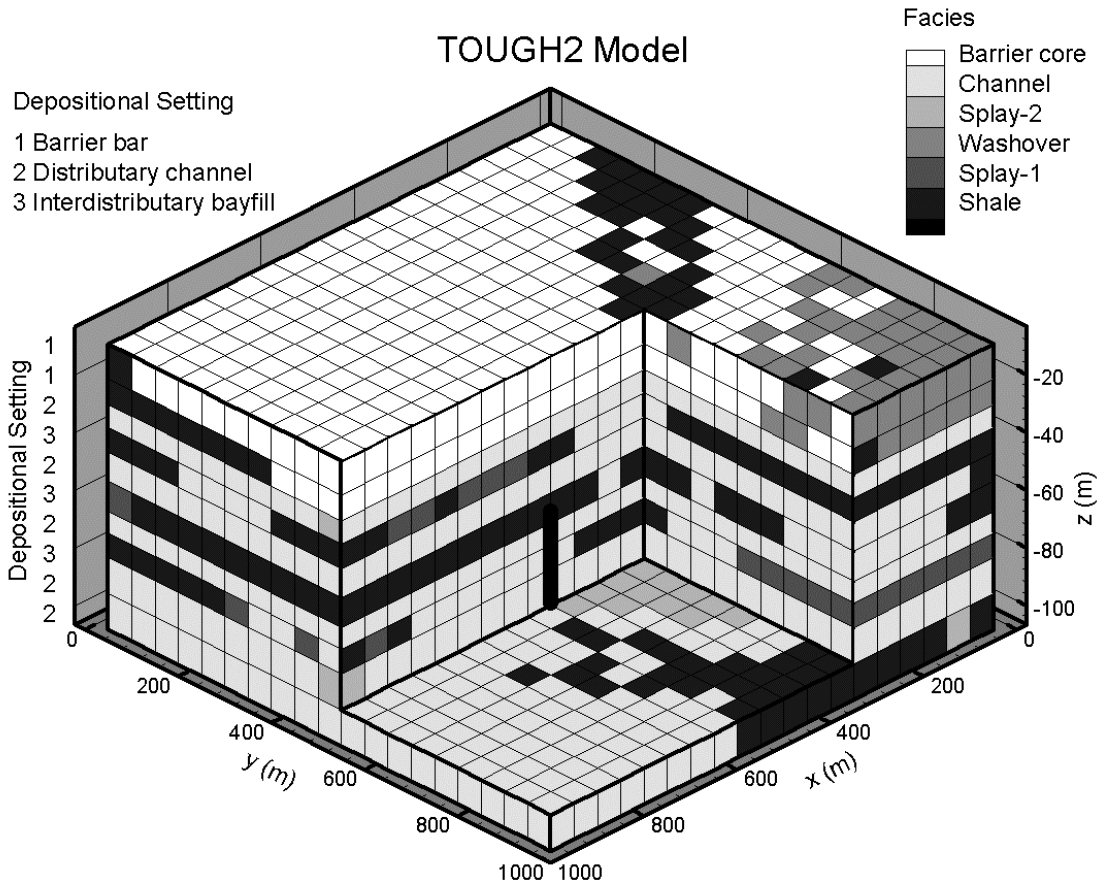

Figure 2. TOUGH2 model of the targeted portion of the Frio formation beneath the Cedar Bayou power plant. The top of the model is at a depth of 1860 m.

Table 1. Model properties.

Facies	Porosity	Horizontal permeability (md)	Vertical permeability (md)
Barrier core	0.32	700	700
Channel	0.30	400	100
Splay-2	0.30	250	100
Washover	0.29	200	50
Splay-1	0.28	150	30
Shale	0.10	0.001	0.0001

Simulation Results

Simulations cover 20 years of CO_2 injection followed by 40 years of recovery. Three cases are considered: the heterogeneous 3D model shown in Figure 2 (the base case), the same model with uniform hydrologic properties (to examine the effect of C_h), and a radial flow model with uniform properties and no gravity (to examine the effects of C_g and the constant pressure boundary).

Heterogeneous 3D Model

Figure 3 shows a series of snapshots of the gas-phase CO_2 distribution during the 20 year injection period, using the model shown in Figure 2. The interplay of gravity and geological heterogeneity leads to a highly irregular CO_2 distribution.

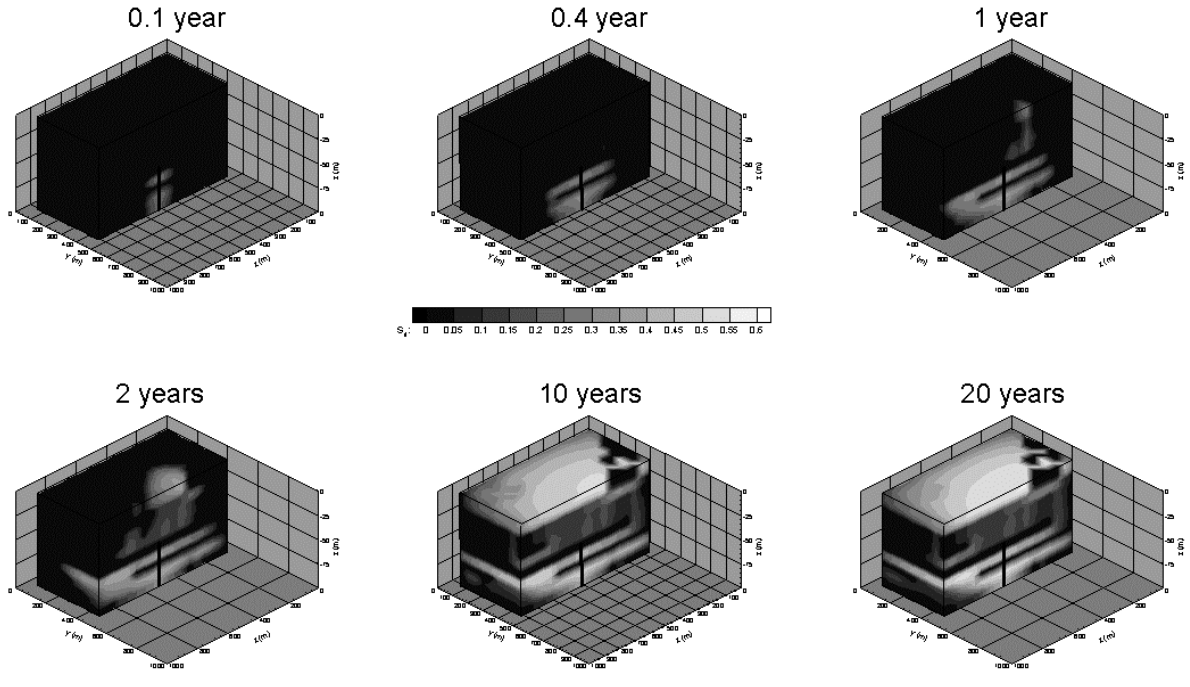

Figure 3. Snapshots of the gas-phase CO_2 distribution during the injection period for the base case.

Figure 4 shows the cumulative masses of CO_2 injected and in place during the 60 year simulation period. These masses are identical until the outer boundary (spill point) of the model is reached after about 1 year of injection. Quasi-steady flow conditions

(approximately equal CO_2 masses injected into the well and leaving the model through the lateral boundaries) develop after about 10 years of injection. Throughout most of the injection period, the phase partitioning of CO_2 into liquid and gas phases remain relatively steady with about 15-20% of the CO_2 dissolved in the aqueous phase. However, after injection ends the mass of CO_2 in the gas phase decreases (leakage out the lateral boundaries), whereas the mass of CO_2 dissolved in the aqueous phase increases slightly.

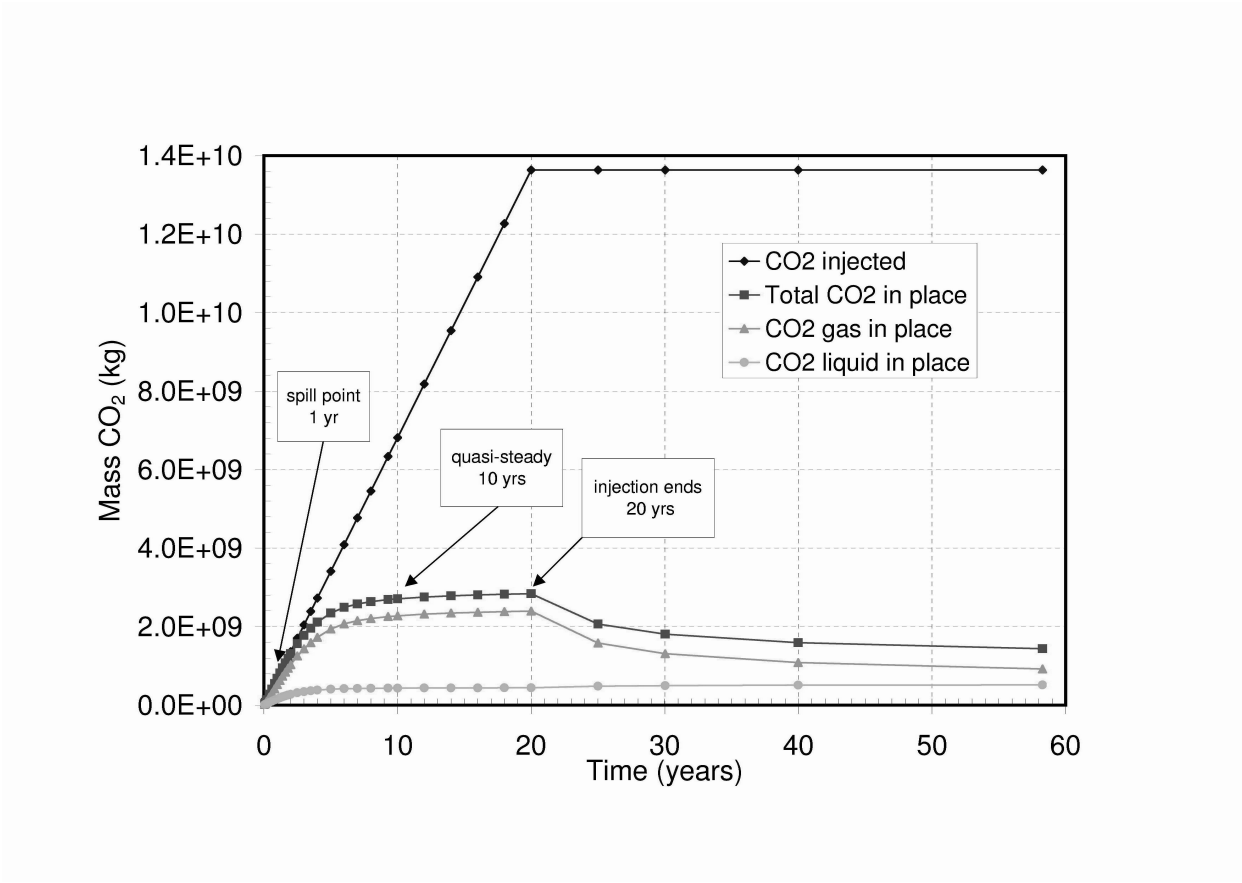

Figure 4. Cumulative CO_2 injected and in place for the heterogeneous 3D model (the base case).

Figure 5 shows capacity C as a function of time, along with the gas-phase and liquid-phase parts of C, $C_{ig}C_gC_h\phi$ and $C_{il}C_gC_h\phi$, respectively. The averaging region is the entire model volume. Note the large increase in capacity (about a factor of four) from the time the spill point is first reached (1 year) to the time when quasi-steady flow conditions are established (10 years). The snapshots of CO_2 distribution shown in Figure 3 illustrate the very different conditions prevailing at these two times. Clearly one must be careful to specify how capacity is defined before drawing conclusions about its value.

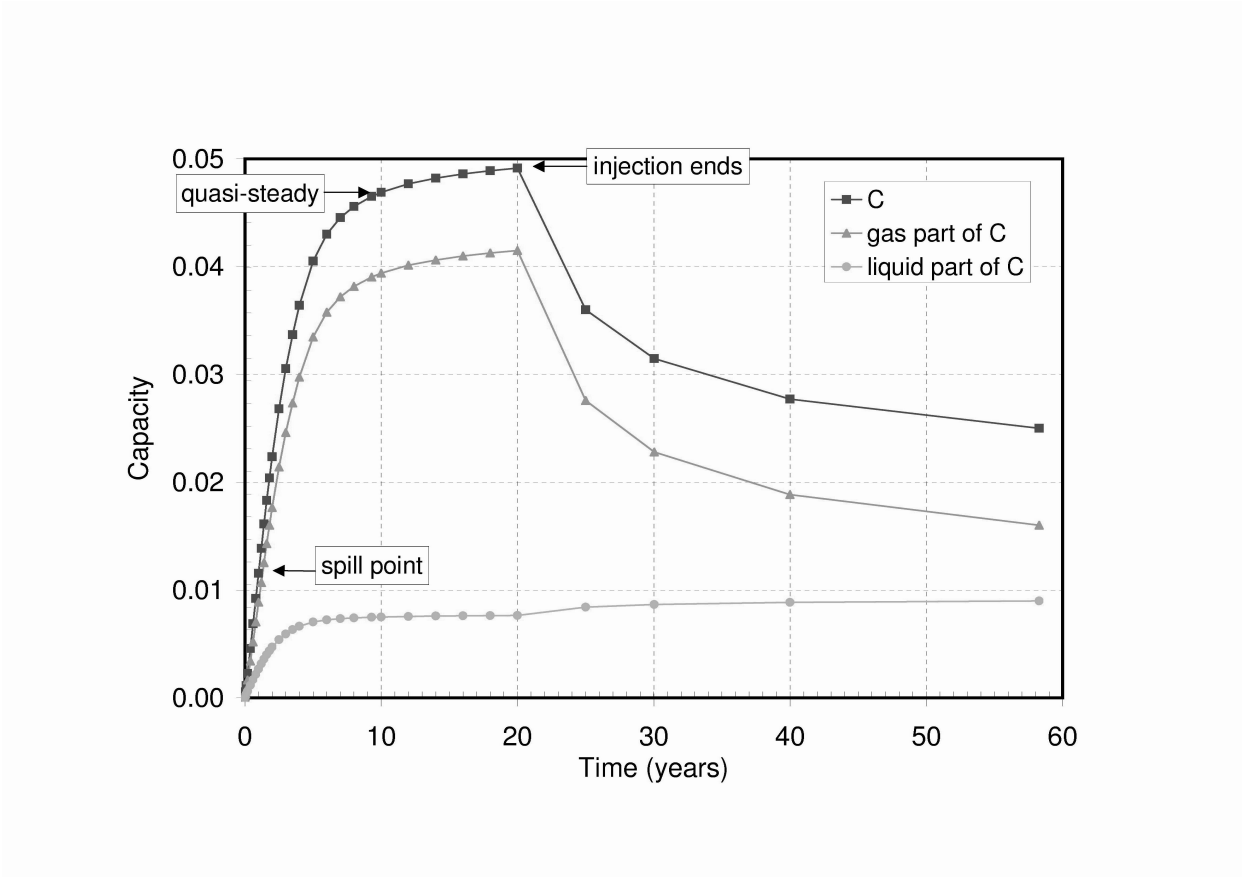

Figure 5. Capacity as a function of time for the heterogeneous 3D model (the base case).

Uniform 3D Model

Figure 6 shows snapshots of the gas-phase CO_2 distribution for a uniform 3D model with the properties of the channel facies given in Table 1. The contrast to the heterogeneous case, Figure 3, is striking. Figure 7 shows the cumulative masses of CO_2 injected and in place and Figure 8 shows the capacity as a function of time. Compared to the heterogeneous case (Figures 4 and 5), the spill point is reached later, but quasi-steady flow regime is reached sooner, and capacity is about 20% smaller. Interestingly, the capacity decreases slightly rather than increasing slightly from the time quasi-steady flow conditions are established until the end of the injection period, reflecting the different flow patterns obtained when gravity acts alone instead of in conjunction with heterogeneity.

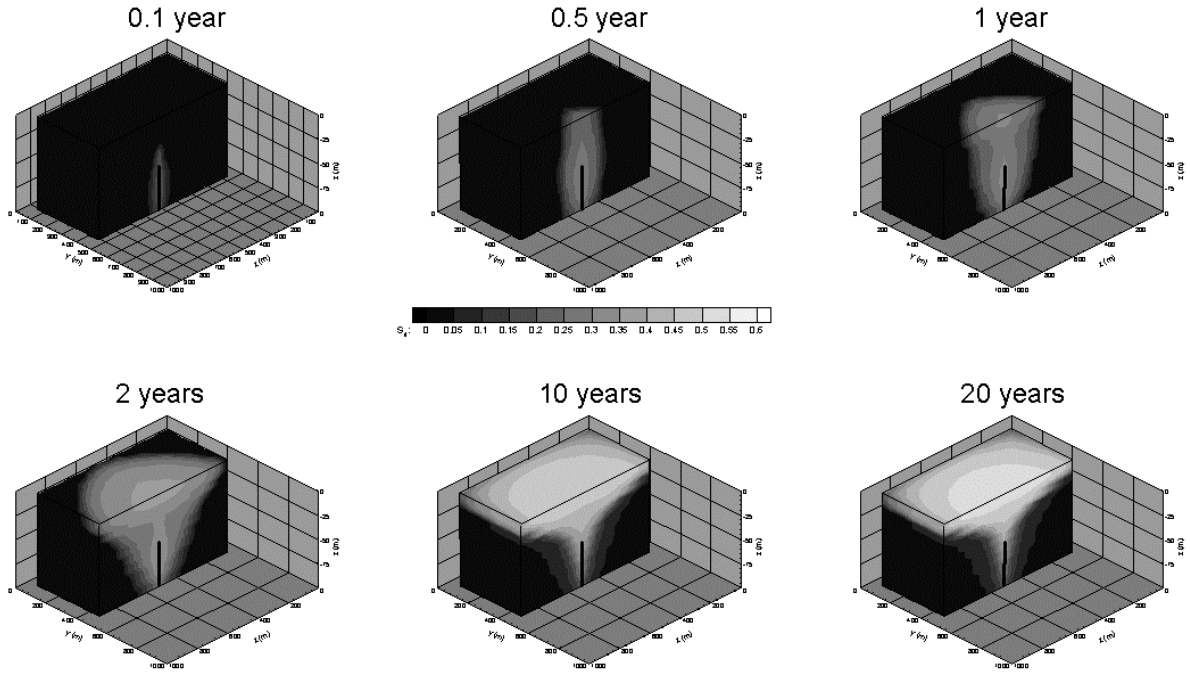

Figure 6. Snapshots of the gas-phase CO_2 distribution during the injection period for the uniform 3D model.

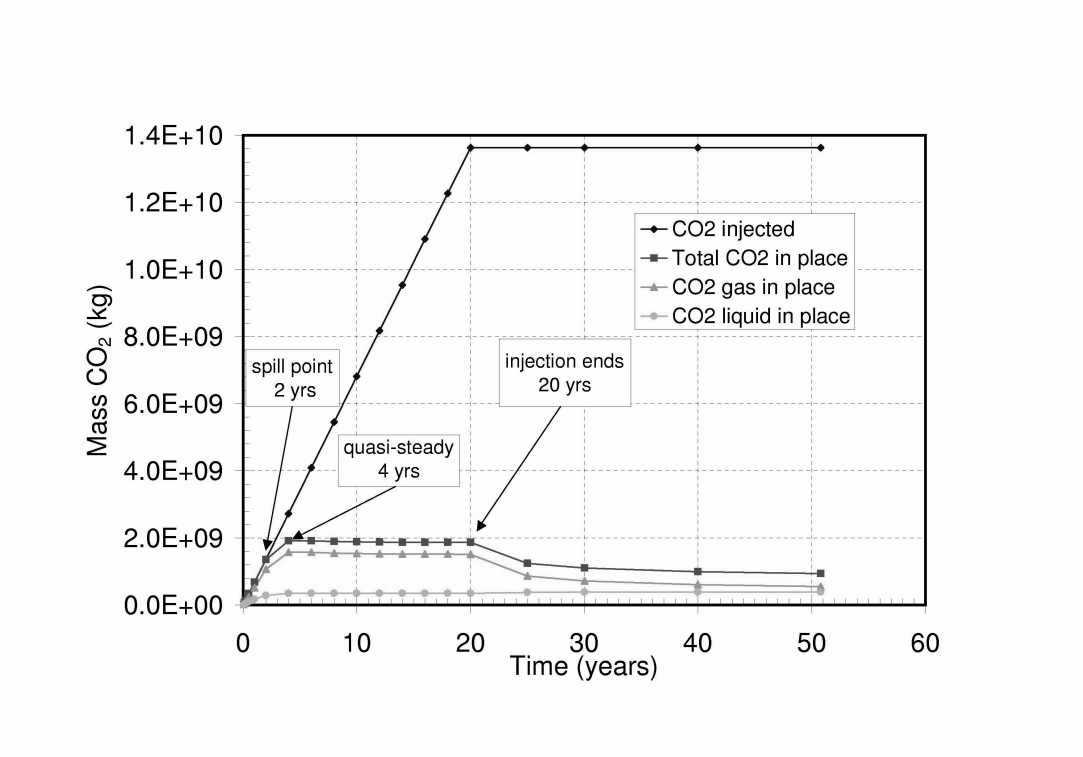

Figure 7. Cumulative CO_2 injected and in place for the uniform 3D model.

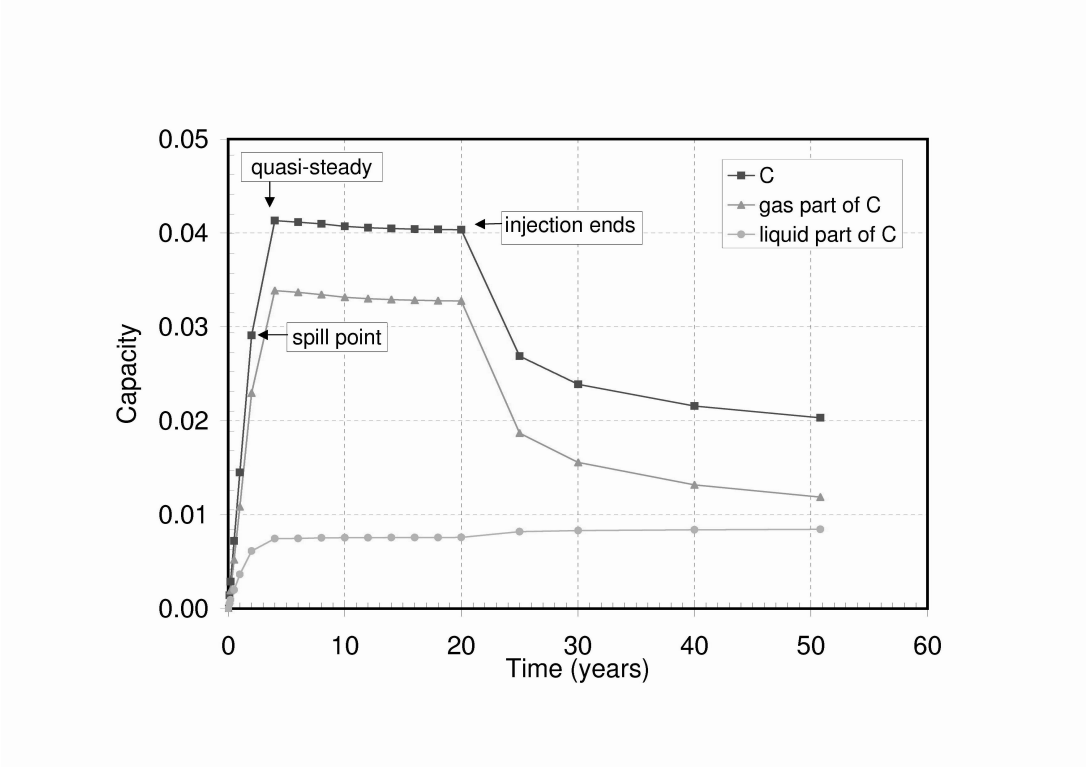

Figure 8. Capacity as a function of time for the uniform 3D model.

Uniform Radial Model

For radial flow geometry and a uniform medium of infinite lateral extent, the flow and transport of injected CO_2 can be described by a similarity variable r^2/t. Because time does not enter the problem independently, capacity will be constant as long as it is defined using the region behind the front as the averaging region. Figure 9 shows profiles of gas saturation S_g, liquid-phase CO_2 mass fraction $X_l^{CO_2}$, and pressure P calculated by TOUGH2 using an essentially infinite radial model with the properties of the channel facies given in Table 1. Averaging behind the CO_2 front yields

$$C_{ig} = \langle S_g \rangle = 0.26 \quad (6)$$

$$C_{il} = \langle S_l X_l^{CO_2} \rho_l / \rho_g \rangle = 0.049. \quad (7)$$

Therefore,

$$C_i = C_{ig} + C_{il} = 0.31 \quad (8)$$

and

$$C = C_i C_g C_h \phi = 0.31 \cdot 0.3 = 0.093, \quad (9)$$

since C_g and C_h are exactly 1 for radial flow.

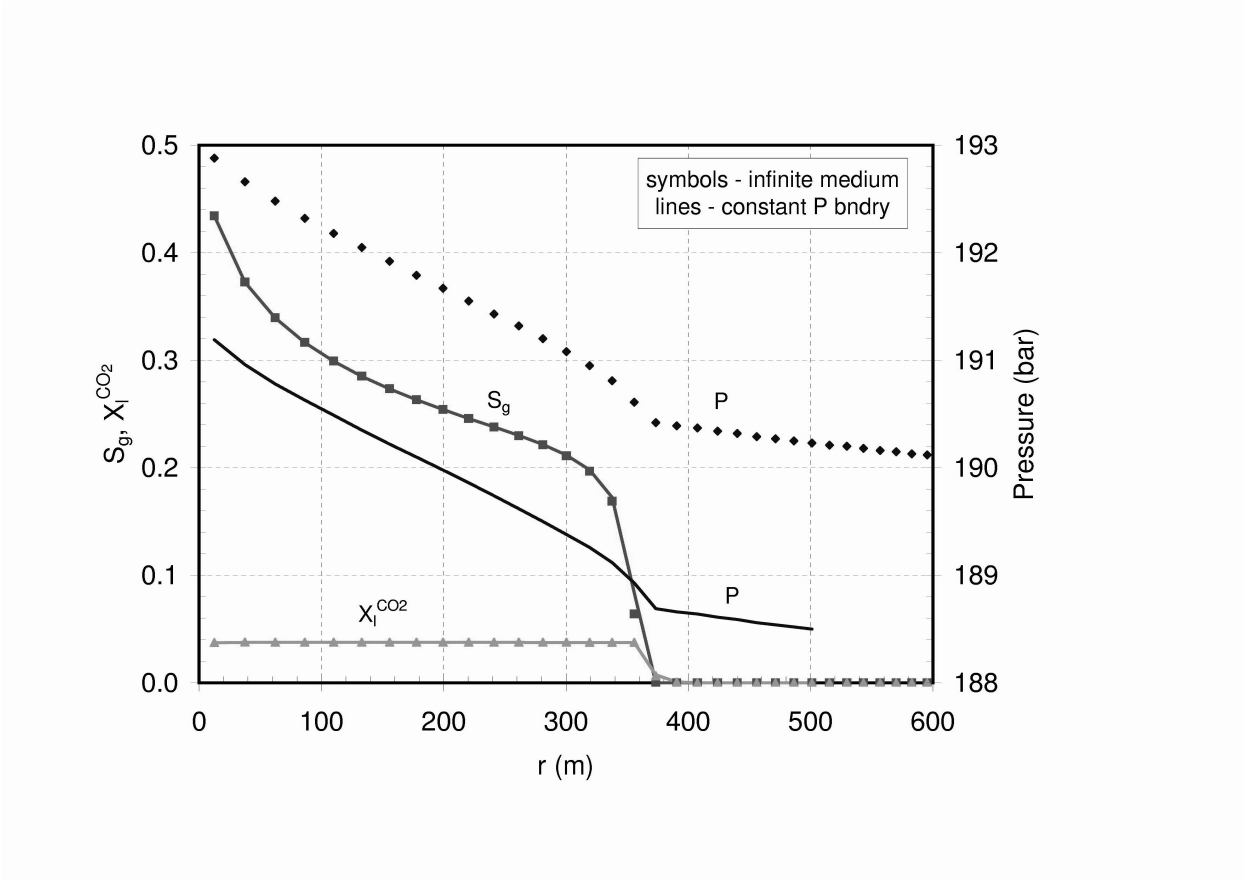

Figure 9. Profiles for uniform radial flow models.

Although mathematically elegant, the similarity solution is limited by not allowing a spill point or a finite duration injection period. With a TOUGH2 numerical model we can examine these effects while maintaining the radial flow geometry with no gravity that is required to isolate C_i.

Figure 9 compares profiles of gas saturation S_g, liquid-phase CO_2 mass fraction $X_l^{CO_2}$, and pressure P for an infinite radial model and a radial model with a constant pressure boundary at a radial distance of r = 500 m. The time of the profiles is 3 years, before the spill point is reached. Only the pressure profile shows an effect of the constant pressure boundary, because the pressure pulse moves away from the injection well much faster than the CO_2 itself does. Gas saturation is insensitive to the boundary conditions, confirming that small-scale models such as that shown in Figure 2 may be used to study the spatial extent and distribution of CO_2 under various conditions, but they are not reliable ways to estimate pressure build up or subsequent recovery.

Figure 10 shows the cumulative masses of CO_2 injected and in place and Figure 11 shows the capacity as a function of time for the radial model with a constant pressure boundary. The spill point and quasi-steady flow states are reached simultaneously, after 6 years of injection. Thereafter, capacity is about the same as for the infinite radial model.

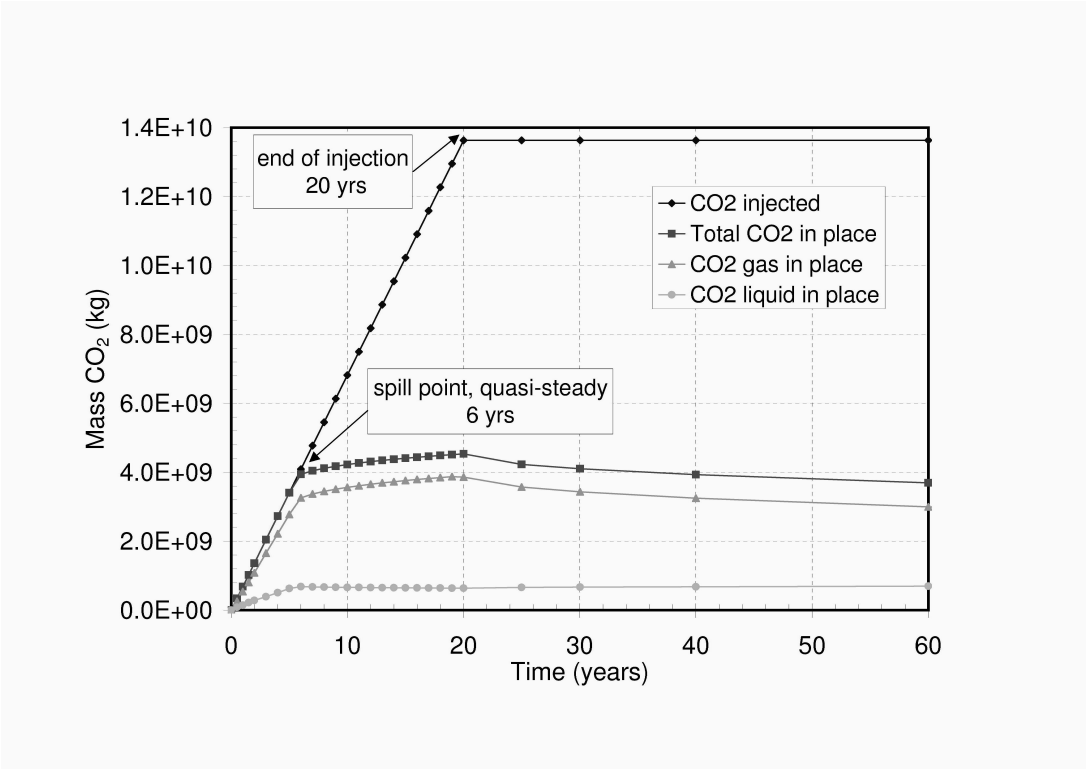

Figure 10. Cumulative CO_2 injected and in place for the uniform radial flow model with a constant pressure boundary.

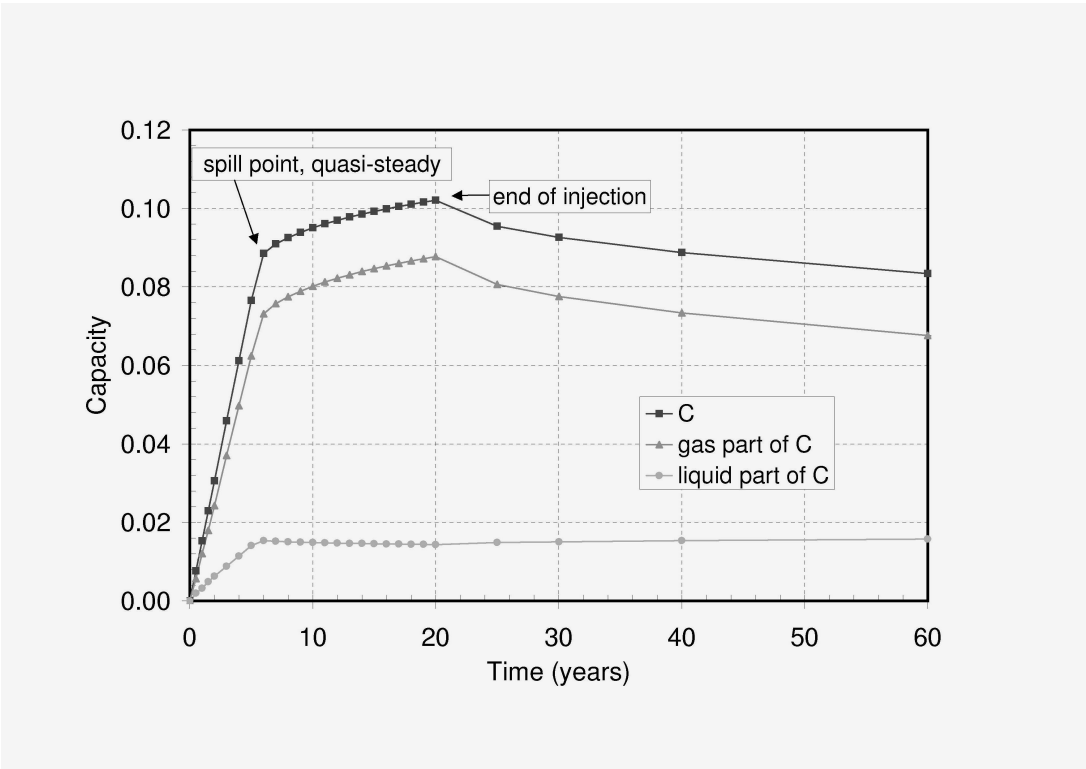

Figure 11. Capacity as a function of time for the uniform radial flow model with a constant pressure boundary.

Table 2 summarizes the capacity factors for the three cases. For the 3D flow cases, the time at which capacity is calculated has a significant effect, with capacity increasing markedly after the spill point is reached. The effects of gravity and heterogeneity counter each other to a certain extent, resulting in similar capacities, especially at later times. Neither 3D case has nearly as large a capacity as obtained for radial flow through a uniform medium, indicating that gravitational forces and formation heterogeneity have a large effect on sequestration capacity. Interestingly, unlike many displacement processes which are affected negatively by heterogeneity, heterogeneity can have a positive effect on sequestration capacity because low permeability layers can counteract the influence of gravity override.

Table 2. Capacity factor summary for Frio formation simulations.

Case	When to evaluate C	C_i	C_g	C_h	ϕ	C (%)
Heterogeneous medium, 3D flow	Spill point	0.06			0.10 to 0.32 (avg 0.21)	1.2
	Quasi-steady	0.22				4.7
	End of injection	0.23				4.9
Uniform medium (channel facies), 3D flow	Spill point	0.10		1	0.30	2.9
	Quasi-steady	0.14		1		4.1
	End of injection	0.13		1		4.0
Uniform medium (channel facies), 1D radial flow, constant pressure boundary	Spill point, quasi-steady	0.30	1	1	0.30	8.9
	End of injection	0.34	1	1		10.2

Table 3 summarizes the capacity factors obtained by other authors, using the present work's conventions and definitions. Neither author includes heterogeneity. By calculating capacity when the spill point is first reached and including gravity, van der Meer (1995) obtains rather low capacities, whereas Pruess et al. (2001) consider the idealized no-gravity, infinite medium case and obtain larger values.

Table 3. Capacity factors determined by other authors (not related to the Frio formation).

		C_i	C_g	C_h	ϕ	C (%)	Comments
van der Meer (1995)	Base case	0.043		0.50 (estimate)	Not given (use 0.12)	0.26	Uniform medium, 2D x,z model, average over trap volume when spill point reached
	Sensitivity studies	0.02 to 0.09		0.50 to 0.75 (estimate)	Not given (use 0.12)	0.12 to 0.81	
Pruess et al. (2001)	Base case	0.35	1	1	0.12	4.2	Uniform medium, radial flow, average behind front when quasi-steady flow established
	Sensitivity studies	0.2 to 0.4	1	1	0.12	2.4 to 4.8	

Conclusions

CO_2 sequestration capacity depends on a combination of factors including multi-phase flow processes, formation and injection well configuration, geologic heterogeneity, and formation porosity. Capacity also depends on the time in the sequestration process at which it is measured: capacity at initial spill point can be much smaller than quasi-steady capacity.

Based on simulation results, the following factors are favorable for sequestration capacity: high intrinsic capacity – which depends on relative permeability to CO_2 and the viscosity ratio (μ_w/μ_{CO2}); high geometric capacity factor – depends on the shape of the structure, permeability anisotropy (k_v/k_h), and the density ratio (ρ_{CO2}/ρ_w); high heterogeneity capacity factor – preliminary indications suggest that layered-type heterogeneities enhance sequestration capacity by counteracting gravitational forces; and high porosity – large pore volume available for sequestration.

Future work to improve the definition of capacity includes running multiple realizations of the Cedar Bayou model, creating and running models of other typical Frio conditions, including heterogeneity within facies, constructing and running larger-scale models, and conducting long-time simulations that include density effects of CO_2 dissolved in liquid water and liquid diffusion.

References

Buckley, S.E. and M.C. Leverett, Mechanism of fluid displacement in sands, *Trans. Am. Inst. Min. Metall. Eng*., 146, 107-116, 1942.

Carle, S.F., A transition probability-based approach to geostatistical characterization of hydrostratigraphic architecture, University of California, Davis, Ph.D. dissertation, 182 p., 1996.

Fogg, G.E., S.F. Carle, and C.T. Green, A connected network paradigm for the alluvial aquifer system, in D. Zhang and C.L Winter, eds., Theory, modeling, and field investigation in hydrogeology: a special volume in honor of Shlomo P. Neuman's 60th birthday, Geological Society of America, Special Paper 348, 2001.

Galloway, W.E., Depositional architecture of Cenozoic gulf coastal plain fluvial systems: The University of Texas at Austin, Bureau of Economic Geology Circular 82-5, 29 p., 1982.

Hovorka, S.D., M.L. Romero, A.G. Warne, W.A. Ambrose, T.A. Trembley, R.H. Trevin□o, and D. Sasson, Sequestration of greenhouse gases in brine formations, http://www.beg.utexas.edu/CO2/, 2000.

Hovorka, S.D., C. Doughty, P.R. Knox, C.T. Green, K. Pruess, and S.M. Benson, Evaluation of brine-bearing sands of the Frio formation, upper Texas gulf coast for geological sequestration of CO_2, First National Conference on Carbon Sequestration, May 14-17, Washington DC, National Energy Technology Laboratory, 2001.

Pruess, K. and J. García. Multiphase Flow Dynamics During CO_2 Injection into Saline Aquifers, *Environmental Geology*, in press, 2001.

Pruess, K., C. Oldenburg, and G. Moridis, TOUGH2 user's guide, version 2.0, Rep. LBNL-43134, Lawrence Berkeley National Laboratory, Berkeley, CA, 1999.

Pruess, K., T. Xu, J. Apps, and J. Garcia, Numerical modeling of aquifer disposal of CO_2, Society of Petroleum Engineers, SPE/EPA/DOE Exploration and Production Environmental Conference, San Antonio, TX, 26-28 February, 2001.

van der Meer, L.G.H., The CO_2 storage efficiency of aquifers, *Energy Conservation and Management*, 36, 6-9, 513-518, 1995.

Vining, M.R., Reserve growth in a mixed sequence of deltaic and barrier-island Frio sandstones: Umbrella Point field, Chambers County, Texas: Gulf Coast Association of Geological Societies Transactions, V. 47, p. 611-619, 1997.

Acknowledgments

We thank Victor Malkovsky of IGEM, Moscow, Russia for kindly providing us with his computer programs of the CO_2 property correlations of V. V. Altunin. We are also grateful to Curt Oldenburg and Stefan Finsterle of Lawrence Berkeley National Laboratory for their technical reviews. This work is part of the GEO-SEQ project, which is supported by the U.S. Department of Energy through the National Energy Technology Laboratory (NETL) under Contract No. DE-AC03-76SF00098.